CMS Physics Analysis Summary

Contact: cms-pag-conveners-b2g@cern.ch 2016/06/12

Search for top quark-antiquark resonances in the all-hadronic final state at $\sqrt{s} = 13$ TeV

The CMS Collaboration

Abstract

A search is presented for the production of heavy resonances decaying to top quark-antiquark pairs in the all-hadronic channel. The analysis is performed using 2.6 fb^{-1} of data collected in proton-proton collisions at $\sqrt{s} = 13$ TeV with the CMS detector. This analysis focuses on high-mass resonances decaying to top quarks with high Lorentz boosts. These highly-boosted top quarks are reconstructed as single jets with substructure corresponding to the t$\rightarrow$bW$\rightarrow$bqq decay. No excess above the expectation from the standard model is observed, and we set limits on the production cross sections of Z′ bosons and RS gluons, for signal models with varying widths. For wider Z′ signal models, we eclipse previous exclusion limits, excluding Z′ bosons with masses up to 3.3 (3.8) TeV, for Z′ widths of 10% (30%) of their masses.

1 Introduction

Many models of new physics predict new particles which have enhanced couplings to the third generation of the Standard Model (SM) [1–9]. Of these, certain models motivate the existence of new heavy resonances that decay to top quark anti-top quark pairs, such as Z′ gauge bosons and Randall-Sundrum Kaluza Klein gluons [10–14]. Recent diphoton and disboson excesses, seen around 750 GeV and 2 TeV by the CMS and ATLAS experiments at the LHC, have provided further motivation for searches for these new heavy bosons [15–17]. In this analysis, we search for heavy resonances in the top quark anti-quark pair production ($\mathrm{t\bar{t}}$) invariant mass spectrum to test for the presence of different new physics models. As benchmark models, we use a leptophobic topcolor model (with the mediator labeled as Z′), as well as Randall-Sundrum Kaluza-Klein gluon production.

Past limits have been set for such resonances, with masses below 900 GeV, by the CDF and D0 experiments at the Tevatron [18, 19]. At the LHC, the CMS and ATLAS experiments have continued to set limits for heavy resonances decaying to $\mathrm{t\bar{t}}$. To do so, the experiments have used data from proton-proton collisions at center of mass energies of 7 and 8 TeV to set increasingly strict limits on resonances above 1 TeV [20–27]. The analyses are categorized by the decay modes of the top quark-antiquark pair, with each top decaying into a b quark and W boson, the W subsequently decaying into leptons or a "jet" of hadrons. Most recently, CMS and ATLAS have released $\mathrm{t\bar{t}}$ resonance limits, using 13 TeV data [28, 29]. Both of these analyses look for one top decaying leptonically and the other hadronically. This analysis also uses 13 TeV data, but looks for events in which both tops decay hadronically.

In the high mass ranges accessible by the LHC at $\sqrt{s} = 13$ TeV, the event topology of $\mathrm{t\bar{t}}$ production requires special techniques. As an example, for Z′ boson masses of more than 1 TeV decaying to $\mathrm{t\bar{t}}$, the produced top quarks will be highly Lorentz boosted and the subsequent $\mathrm{t} \to \mathrm{b}W \to \mathrm{bqq}$ decays will usually merge together to form a single jet with substructure. We utilize special reconstruction techniques to identify these "boosted top quarks", namely the CMS Top Tagger (V2) [30], which utilizes the modified mass drop tagger [31], N-subjettiness [32, 33], and subjet b-tagging algorithms [34] to identify jets from boosted top quarks.

The analysis utilizes the differences in the invariant mass spectrum of the $\mathrm{t\bar{t}}$ pairs ($M_{\mathrm{t\bar{t}}}$) from resonant and non-resonant SM production in order to search for new resonances. The dominant background from non-top multijet backgrounds (NTMJ) is estimated from data. It is an update to two existing CMS searches ($\sqrt{s} = 7$ TeV [20] and $\sqrt{s} = 8$ TeV [24]). The updated search uses the 13 TeV dataset collected in 2015, corresponding to an integrated luminosity of 2.6 fb^{-1}, with new t-tagging tools and subjet b-tagging.

2 CMS detector and reconstruction

The central feature of the CMS apparatus [35] is a superconducting solenoid of 6 m internal diameter, providing a magnetic field of 3.8 T. Within the superconducting solenoid volume are a silicon pixel and strip tracker, a lead tungstate crystal electromagnetic calorimeter (ECAL), and a brass/scintillator hadron calorimeter (HCAL). Muons are measured in gas-ionization detectors embedded in the steel return yoke outside the solenoid. Extensive forward calorimetry complements the coverage provided by the barrel and endcap detectors.

The event reconstruction is based on the CMS Particle Flow (PF) algorithm [36, 37], which takes into account information from all subdetectors, including charged particle tracks from

the tracking system, energy deposits in the electromagnetic and hadronic calorimeters and tracks reconstructed in the muon chambers. Given this information, all particles in the event are reconstructed as electrons, muons, photons, charged hadrons or neutral hadrons.

Muon and electron candidates are only used to veto events with a lepton to be statistically independent from searches for $\bar{t}t$ resonances involving leptons.

Hadronic jets are clustered from particle flow algorithm particle inputs with the anti-k_T algorithm [38] using the FASTJET 3.0 software package [39, 40] with $R = 0.8$ (AK8 jets). Charged hadrons associated with pileup vertices are not considered when clustering. Corrections based on the jet area [41] are applied to the jets to remove the energy contribution of neutral hadrons arising from pileup collisions. Further corrections are used to account for the nonlinear calorimetric response, as a function of η and p_T [42], derived from simulation and data-to-simulation correction factors. All AK8 jets are required to have $p_T > 400$ GeV and rapidity $|y| < 2.4$. Spurious jets due to detector noise effects are removed by requiring at least 1% of the jet energy to come from the electromagnetic and hadronic calorimeters.

These AK8 jets are then taken as top quark candidates (t-jets). To identify the jets as t-jets, the "CMS Top Tagger V2" algorithm is used. In this algorithm, the constituents of the AK8 jets are reclustered using the Cambridge-Aachen algorithm [43, 44]. The modified mass drop tagger (MMDT) algorithm [31], also known as the "soft drop" algorithm with angular exponent $\beta = 0$, soft threshold $z_{cut} < 0.1$, and characteristic radius $R_0 = 0.8$ [45], is used to remove soft, wide-angle radiation from the jet. This algorithm is also used to identify two subjets within the AK8 jet. The subjet corresponding to the b-quark can be identified using subjet b-tagging techniques as in Refs. [26, 46]. Specifically, the Combined Secondary Vertex v2 (CSVv2) algorithm is used to identify b-tagged subjets. A 'medium' working point of the algorithm is used, which provides an efficiency of approximately 70% for the identification of real b jets, while rejecting 99% of light-flavor jets. To identify the three-pronged substructure of the hadronically-decaying top quark, the N-subjettiness variable τ_3/τ_2 (abbr. τ_{32}) [32, 33] is used. This variable is calculated using all particle flow inputs to the AK8 jet, with N-subjettiness axes defined by the one-pass minimization procedure [33].

The specific working point used in this analysis is defined by requiring that the soft-dropped mass satisfy $110 < M_{SD} < 210$ GeV and the N-subjettiness variable satisfy $\tau_{32} < 0.69$, which corresponds to a misidentification rate in simulation of 3% [30]. Jets satisfying the jet mass and N-subjettiness selections are referred to as "t-tagged". Additionally, "t-tagged" jets are considered to have a subjet b-tag if they contain at least one soft-drop subjet with CSVv2 discriminant satisfying the 1% mistag rate working point.

3 Data and simulation samples

The data were collected with an online trigger that required the sum of the jet activity of the event (H_T) to be larger than 800 GeV. The trigger selection is over 95% efficient when the offline H_T is larger than 1000 GeV. This offline requirement has little effect on the signal acceptance, due to the large resonance masses. The dataset analyzed corresponds to an integrated luminosity of 2.6 fb^{-1}.

Several simulated signal samples were analyzed. Using MADGRAPH v5.2 [47], we generated neutral spin-1 resonances (Z′) with the same couplings as the SM Z boson to left- and right-handed fermions. This is referred to as the "Sequential Standard Model" (SSM). In this analysis only Z′ decaying to $\bar{t}t$ quark pairs are considered. We use three arbitrarily-defined widths of

1%, 10%, and 30%. These were chosen to be smaller than, comparable to, and larger than the intrinsic detector resolution (respectively). Z' samples with resonance masses between 1 TeV and 4 TeV were generated. Higher-order parton radiations were calculated for up to three extra partons at tree-level. The parton showering was modeled with PYTHIA 8.2 [48], and the MLM algorithm [49] was used for the matching. The leptophobic topcolor model is assumed to have similar event characteristics as the SSM Z'.

In addition to the SSM model, one specific additional model was chosen, where a Kaluza–Klein Randall–Sundrum gluon was produced with PYTHIA 8.2. This nearly always results in resonant $\mathrm{t\bar{t}}$ production, with a nontrivial width defined by the physics of the model. Kaluza–Klein gluon excitations are generated with resonance masses between 1 TeV and 4 TeV. The branching ratio of the resonance state into top quark pairs is about 94%, with the remaining fraction decaying mostly to bottom quark pairs.

Top quark pair events, produced in the SM via the strong interaction, are generated with the next-to-leading-order generator POWHEG [50–54]. The $\mathrm{t\bar{t}}$ sample is normalized to $\sigma_{\mathrm{t\bar{t}}} = 831.76$ pb [55], but is eventually extracted from the sample in situ in a likelihood fit. All samples are interfaced to PYTHIA 8.2 for parton showering.

Simulated QCD multijet events are used for validation of the background estimation procedure but are not used when performing the search (the multijet background is estimated from sideband regions in data). We use multijet events generated with PYTHIA 8.2, binned in the H_{T} of the hard scatter to increase MC statistics in the high-energy region.

All events were generated with the NNPDF 3.0 PDF sets [56]. Whenever PYTHIA 8.2 is used for showering and hadronization, the underlying event tune CUETP8M1 has been used [57]. All simulated samples include the simulation of additional inelastic proton-proton interactions within the same bunch crossing ("in-time pileup") and the simulation of additional contribution in the signal readout from the previous and next bunch crossing ("out-of-time pileup") which are assumed to be 25 ns apart from the main bunch crossing. Simulated events are reweighted to match the observed distribution of the number of pileup interactions in data, based on a minimum bias cross section of 69 mb.

4 Event selection and background estimation

The event topology considered in this analysis is dijets that both satisfy kinematic and t-tagging selection criteria. Both jets are required to have $p_{\mathrm{T}} > 400$ GeV, $|y| < 2.4$, and both are required to be t-tagged. A back-to-back topology is selected by requiring the azimuthal angles of the two leading jets to satisfy $|\Delta\phi| > 2.1$. Furthermore, the scalar sum of all of the jets in the event is required to satisfy $H_{\mathrm{T}} > 1000$ GeV to be above the trigger threshold.

Events are further categorized into six regions (A-F) based on two criteria: (1) the rapidity difference ($|\Delta y|$) between the two AK8 jets; and (2) the number of jets with at least one b-tagged subjet (considering only the two highest p_{T} jets).

This analysis has two primary sources of background, non-top multijet (NTMJ) and SM $\mathrm{t\bar{t}}$ events.

The estimate for $\mathrm{t\bar{t}}$ events is taken from simulation to model the shape of the $m_{\mathrm{t\bar{t}}}$ distribution. The normalization of this distribution is initially set to the theoretical cross section, but is allowed to vary within both rate and shape uncertainties during limit setting. The shape and normalization are both fitted and extracted from the six event categories. The variation pre-

dominantly affects categories C and F, which require two subjet b-tags, and thus have a large SM $t\bar{t}$ contribution.

We apply corrections to $t\bar{t}$ and signal events due to differences in selection efficiencies measured in data and simulated events. For the top-tagging efficiency, we select a sample enriched in $t\bar{t}$ events using a muon+jets topology. The scale factor (SF), or ratio of efficiencies measured in data and simulation, is found to be 0.81 ± 0.08 for the t-tagging criteria described above. This scale factor is used to weight events used in the analysis, applied once per t-tagged jet in all simulated events. Scale factors for subjet-b-tagging efficiencies, having both p_T and η dependence, are applied independently from the t-tagging scale factors. The subjet-b-tagging efficiencies range from 95 to 100% for the p_T range considered here.

For the NTMJ estimate, we use a data-driven technique. This technique is similar to that described in Ref. [26]. The method involves selecting a sample with low SM $t\bar{t}$ contribution by inverting the t-tagging N-subjettiness requirement on one selected jet (anti-tag) and determining the t-tagging rate for the second jet (probe). The anti-tagged jet is required to satisfy $110 < M_{SD} < 210\,\text{GeV}$ and $\tau_{32} > 0.69$. This 'anti-tag and probe' method yields a per-jet mistag rate parameterized as a function of jet momentum and is measured separately for events falling into each of the six b-tag and $|\Delta y|$ categories (Fig. 1). The method is designed such that it selects a sample in data dominated by NTMJ events. A small number of real $t\bar{t}$ events survives this selection. This contamination is removed by subtracting the distributions measured in $t\bar{t}$ simulation from those measured in the anti-tag and probe selection in data.

Once the mistag rate is determined from the NTMJ control sample, it is used to estimate the normalization and shape of NTMJ events passing the final event selection. To do this, we use a "singly-tagged" region that contains events with at least one t-tagged jet. In order to avoid bias, we randomly select one of the two leading top jet candidates and require that it passes the t-tagging selection described above. If the randomly chosen jet is t-tagged, we include this event and weight it by the appropriate mistag rate based on the momentum of the jet opposite the tagged jet, the rapidity difference, and the number of subjet b-tags.

Using this single-tagged control region without any requirements on the second jet leads to an overlap between the signal region and this region used to estimate the multijet background. To remove the effects of double-counting, the $t\bar{t}$ contribution is subtracted from the multijet estimate. This is done by evaluating the mistag weighting procedure described above on the simulated $t\bar{t}$ events, to find the contribution of $t\bar{t}$ events that would enter the NTMJ estimate when applying the method using data. This contribution is subtracted from the NTMJ estimate, accounting for a $t\bar{t}$ contamination of about 1–2% of the NTMJ background estimate in the 0 b-tag event regions, and about 6–10% in the other regions.

As a final step to the shape determination of the NTMJ estimate, we account for the fact that the second jet, having no tag selection applied, will have different kinematics than those jets in the signal region. To mimic the kinematics of the signal region, we randomly set the mass of this second jet according to a distribution of jet masses from simulated QCD events in the same window used for the signal region selection, $110 < M_{SD} < 210$ GeV. This method is validated using simulated QCD events.

5 Systematic Uncertainties

Several sources of systematic uncertainty affect both the overall normalization of the background components in the analysis, as well as the shapes of the $t\bar{t}$ invariant mass ($m_{t\bar{t}}$) dis-

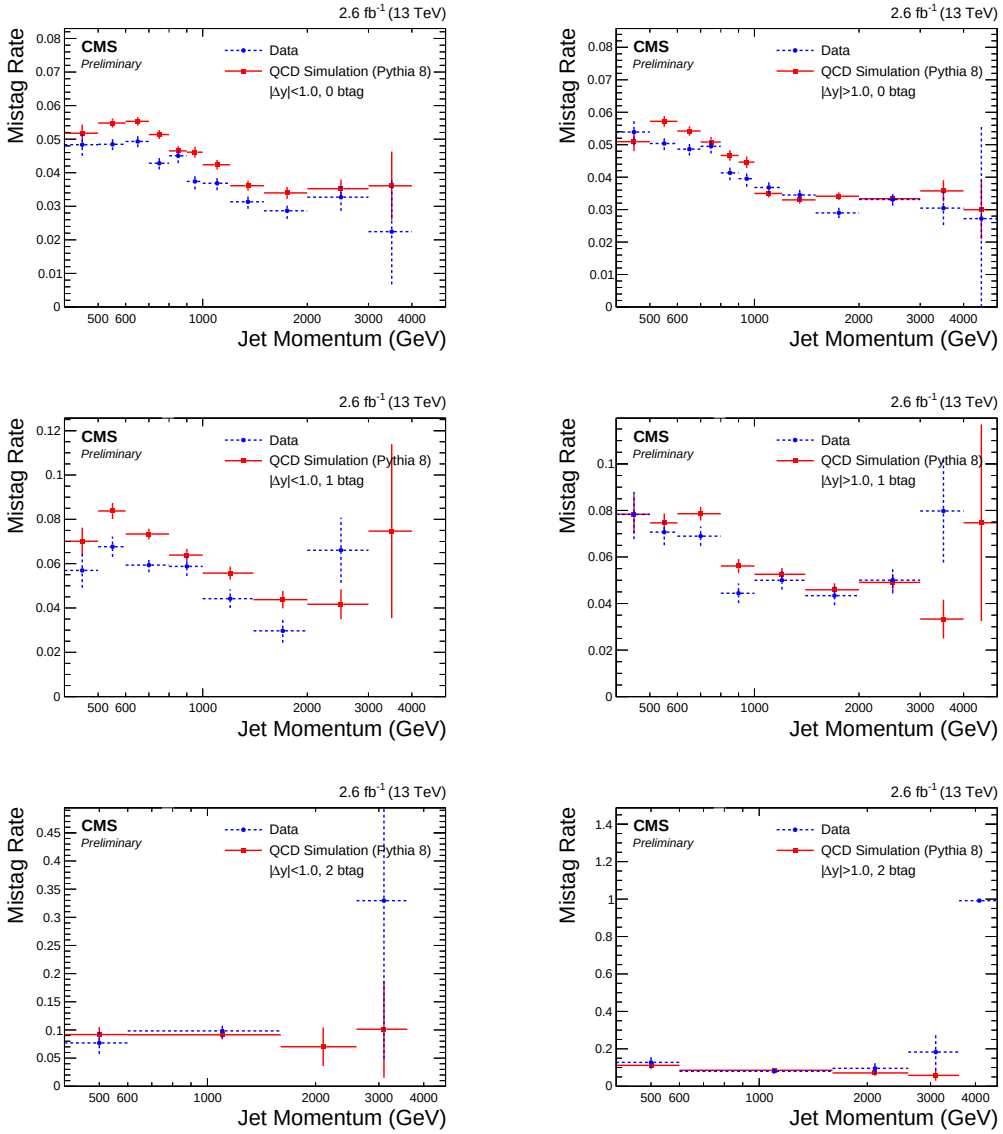

Figure 1: t-tagging mistag rate as measured with an anti-tag and probe procedure. The red squares indicate the mistag rate measured in QCD simulation. Blue circles indicate the mistag rate measured in data. The contamination from $t\bar{t}$ is removed by subtracting simulated $t\bar{t}$ events, normalized to expectation. The mistag rate is measured separately for each of the six event categories described in the text.

Table 1: Summary of systematic uncertainties applied to the analysis.

Systematic Uncertainty Source	Value	Type
Jet b-tag Efficiency	$\pm 1\sigma$	Rate + Shape
Jet t-tag Efficiency	20%	Rate
Jet Energy Scale	$\pm 1\sigma$	Rate + Shape
Jet Energy Resolution	$\pm 1\sigma$	Rate + Shape
Integrated Luminosity Measurement	2.7%	Rate
Parton Distribution Functions	$\pm 1\sigma$	Rate + Shape
Pileup Reweighting	$\pm 1\sigma$	Rate + Shape
Mistag Rate Measurement	$\pm 1\sigma$	Rate + Shape
$t\bar{t}$ Matrix Element Scale	$\pm 1\sigma$	Rate + Shape
$t\bar{t}$ Parton Shower Scale	$\pm 1\sigma$	Rate + Shape
$t\bar{t}$ Cross Section	15%	Rate
NTMJ Jet Kinematics	$\pm 1\sigma$	Rate + Shape
NTMJ Closure Test	$\pm 1\sigma$	Rate + Shape

tribution for signal and background processes. These are treated as nuisance parameters in the likelihood fit as described in the next section, and hence will be constrained, if possible, using the observed data. The input distributions and values for the uncertainties on the nuisance parameters are determined as described below. Table 1 shows a list of the systematic uncertainties.

We evaluate the effect of the jet energy scale uncertainty on the simulated samples. This is done by varying the jet four-momentum up and down by the jet energy scale uncertainty, which varies as a function of jet p_T and pseudorapidity. This affects the shape of the $m_{t\bar{t}}$ distribution and changes the overall normalization by up to approximately 5%.

We account for differing jet energy resolutions between simulated events and data events. We smear the jet momentum four-vectors by an additional (η-dependent) 6-12%. We assume that the jet energy resolution for subjets is the same as that for the hard jets. The variation of the subjet p_T is also included in these shape uncertainties. This results in negligible shape and normalization changes in the $m_{t\bar{t}}$ distribution, relative to other effects.

We vary the minimum bias cross section used to reweight simulated events based on the number of pileup interactions by 5%, resulting in shape differences in the $m_{t\bar{t}}$ spectrum.

The uncertainties related to SM $t\bar{t}$ events include several contributions: a rate-only component due to the uncertainty in the $t\bar{t}$ cross section, which is taken to be 15% [58], a shape component for uncertainties in the renormalization and factorization scale (Q^2), and parton shower uncertainties. The Q^2 shape uncertainties are implemented by reweighting $t\bar{t}$ events using several independent variations of the renormalization (μ_R) and factorization (μ_F) scales by up to one-half or two times the nominal value, and taking the envelope of the resulting $m_{t\bar{t}}$ distributions as the systematic shape variation. Additionally, we explore the effect of initial and final state radiation on the reconstruction of the $t\bar{t}$ system. An uncertainty is derived by using $t\bar{t}$ events generated with different Q^2 scales used for the parton shower generation and evolution in simulation. This uncertainty is applied as a shape template on the reconstructed $m_{t\bar{t}}$ distribution.

We evaluate the effects of the choice of parton distribution function (PDF) on the simulated samples. The shape uncertainties are obtained by reweighting the simulated events using different variations of the eigenvectors used in the simulation. The weights for each variation are added in quadrature to obtain a combined shape and normalization uncertainty due to PDF

Table 2: Expected background and observed data yields for the six event categorizations used in the final analysis selection. Errors include both the statistical and systematic components.

	$\|\Delta y\| > 1.0$		
Process	**0 b-tags**	**1 b-tag**	**2 b-tags**
NTMJ	1291 ± 23	371 ± 12	31 ± 5.9
SM $t\bar{t}$	47 ± 9.4	82 ± 13	37 ± 7.9
Total Background	1338 ± 24	454 ± 17	68 ± 10
DATA	1300	441	78

	$\|\Delta y\| < 1.0$		
Process	**0 b-tags**	**1 b-tag**	**2 b-tags**
NTMJ	1321 ± 41	402 ± 14	36 ± 8.9
SM $t\bar{t}$	75 ± 16	142 ± 25	72 ± 17
Total Background	1396 ± 44	544 ± 29	108 ± 19
DATA	1414	596	124

effects.

The mistag rate uncertainty, shown in Fig. 1, contains statistical uncertainties that are propagated to the NTMJ background estimation. Additionally, the systematic uncertainty associated with the 'mass-modified' procedure, which is used to correct the kinematic bias in the background estimation, is computed by taking half the difference between the uncorrected background estimate and the 'mass-modified' background estimate. This affects the shape and normalization of the $m_{t\bar{t}}$ distribution. Simulated QCD events are used in a closure test to verify that the background estimation procedure accurately predicts the double t-tagged $m_{t\bar{t}}$ distribution. An additional systematic uncertainty is assigned to the NTMJ background estimate based on small disagreements (up to 10%) observed in the shape of the kinematic threshold at low $m_{t\bar{t}}$ values in this closure test.

6 Statistical interpretation and results

The expected background is a combination of NTMJ events, as estimated from data, and simulated $t\bar{t}$ events. Jet kinematic variables are well modeled by the expected background. Table 2 shows the expected background yields for the six analysis categories used, along with the observed number of data events and the background expected from the SM.

The distributions of $m_{t\bar{t}}$ used for signal discrimination in each of the six event categories are shown in Fig. 2. We do not observe any significant excess of events above the expected background from SM $t\bar{t}$ and NTMJ events. We extract limits on the cross sections of the signal model hypotheses considered for this analysis.

We perform a template-based shape analysis with the Theta software package [59], using these $m_{t\bar{t}}$ distributions. A Bayesian likelihood-based method is used, allowing the expected background model to fluctuate within the various systematic and statistical uncertainties to find the best fit to the observed data distribution. Each systematic uncertainty is accounted for with an individual nuisance parameter in the likelihood formation. For the signal cross section parameter, we use a uniform prior distribution. For the other nuisance parameters, a lognormal prior distribution is used. By varying these parameters within their prior distribution func-

Table 3: Observed and expected exclusion ranges for resonance masses in each of the signal models tested in the analysis.

Mass Exclusion Limits

Signal Model	Exclusion Ranges (TeV)	
	Expected	Observed
Z′ (1% Width)	1.2 – 1.6	1.4 – 1.6
Z′ (10% Width)	1.0 – 3.1	1.0 – 3.3
Z′ (30% Width)	1.0 – 3.7	1.0 – 3.8
RS Gluon	1.0 – 2.5	1 – 2.4

Table 4: Table of expected and observed 95% CL cross section limits, for the narrow (1% width) Z′ signal hypothesis.

Z′ (1% Width) Signal Hypothesis

Mass (GeV)	Observed 95% CL Limit (pb)	Expected 95% CL Limits (pb)				
		-2σ	-1σ	Median	$+1\sigma$	$+2\sigma$
1000	**12**	7.9	11	**16**	25	39
1250	**2.4**	0.74	1.0	**1.5**	2.2	3.0
1500	**0.6**	0.34	0.47	**0.68**	0.98	1.4
2000	**0.29**	0.14	0.19	**0.27**	0.39	0.56
2500	**0.18**	0.076	0.099	**0.15**	0.21	0.3
3000	**0.087**	0.065	0.086	**0.12**	0.18	0.25
3500	**0.061**	0.058	0.075	**0.11**	0.16	0.23
4000	**0.059**	0.053	0.071	**0.1**	0.15	0.31

tions, pseudoexperiments are performed to estimate the 68% and 95% CL (1- and 2-sigma) expected limit bands.

Figures 3 show the expected cross section limits obtained from the analysis for the four different signal hypotheses, using the combination of the six independent signal regions A-F. The Z′ cross section is calculated at next-to-leading order (NLO) from the leptophobic topcolor model. The RS KK gluon signal cross section is calculated from leading order (LO) PYTHIA 8 and a scale factor of 1.3 is applied to take into account the ratio of NLO to LO predictions [60]. The cross section and resonance mass exclusions are also shown numerically in Tables 3 – 7.

7 Conclusions

We have performed the first search for top quark pair resonances in the all-hadronic channel using $\sqrt{s} = 13$ TeV data from the LHC Run 2. The search uses a new top-tagging algorithm, optimized for Run 2 analyses, using the jet mass from the modified mass-drop tagger and N-subjettiness jet substructure variables along with subjet b-tagging. We estimate the non-top multijet background using a mistag rate measured in a control region depleted of $\mathrm{t\bar{t}}$ events. No excess above the standard model expectation is observed, and we set limits on the production cross sections of Z′ bosons and RS gluons, for signal models with varying widths. For some signal models, we eclipse previous exclusion limits, excluding Z′ bosons with masses up to 3.3 (3.8) TeV, for Z′ relative widths of 10% (30%) of their masses.

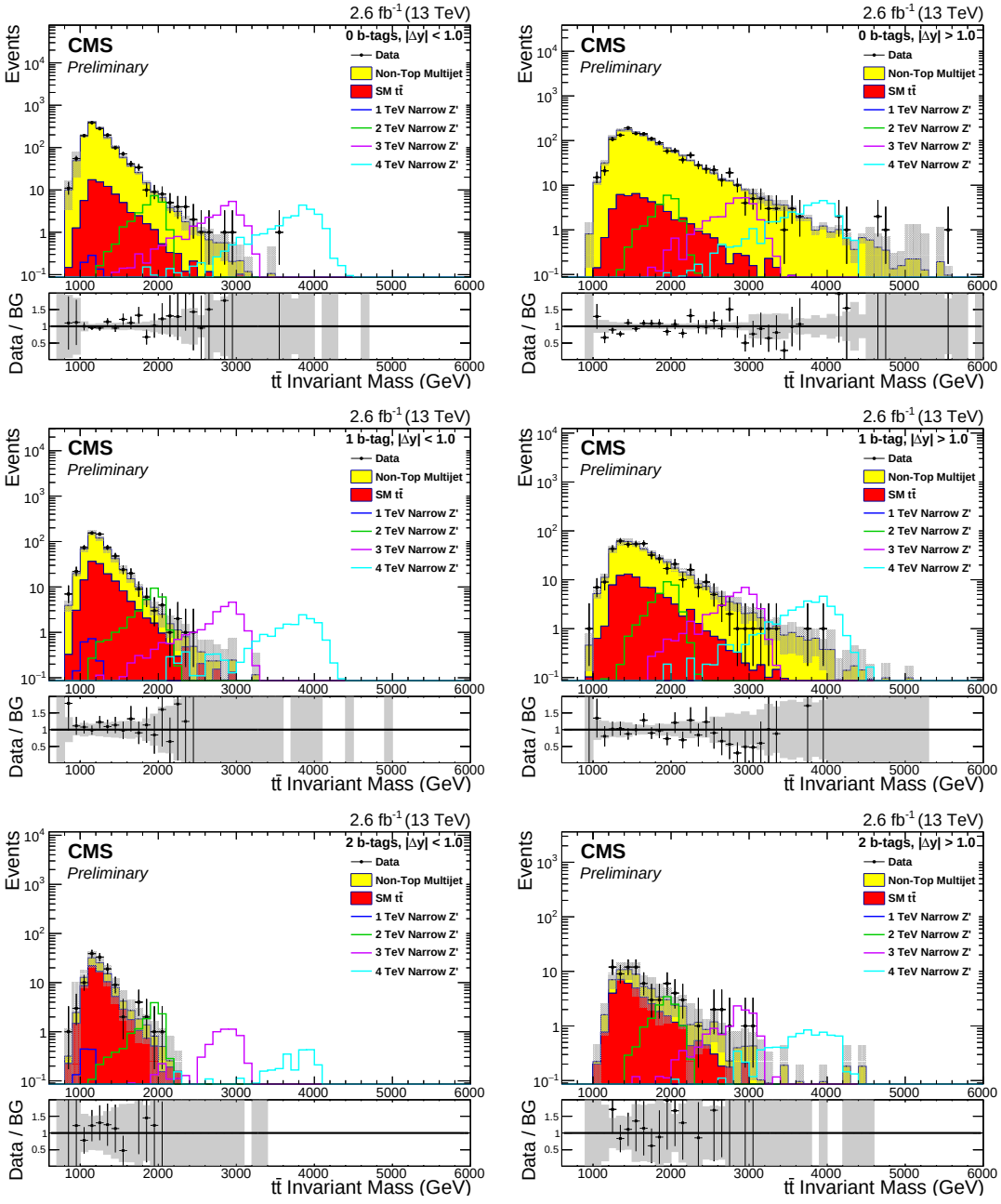

Figure 2: Final log-scale distributions of $m_{\mathrm{t\bar{t}}}$ for all six signal regions, with the $\Delta y < 1.0$ categories shown in the left column and the $\Delta y > 1.0$ categories in the right. The number of b-tags in the plots increase from zero in the first row to two b-tags in the third row. The shaded region corresponds to the combined systematic and statistical uncertainties on the background model. Signal models have been normalized to a cross section of 1 pb.

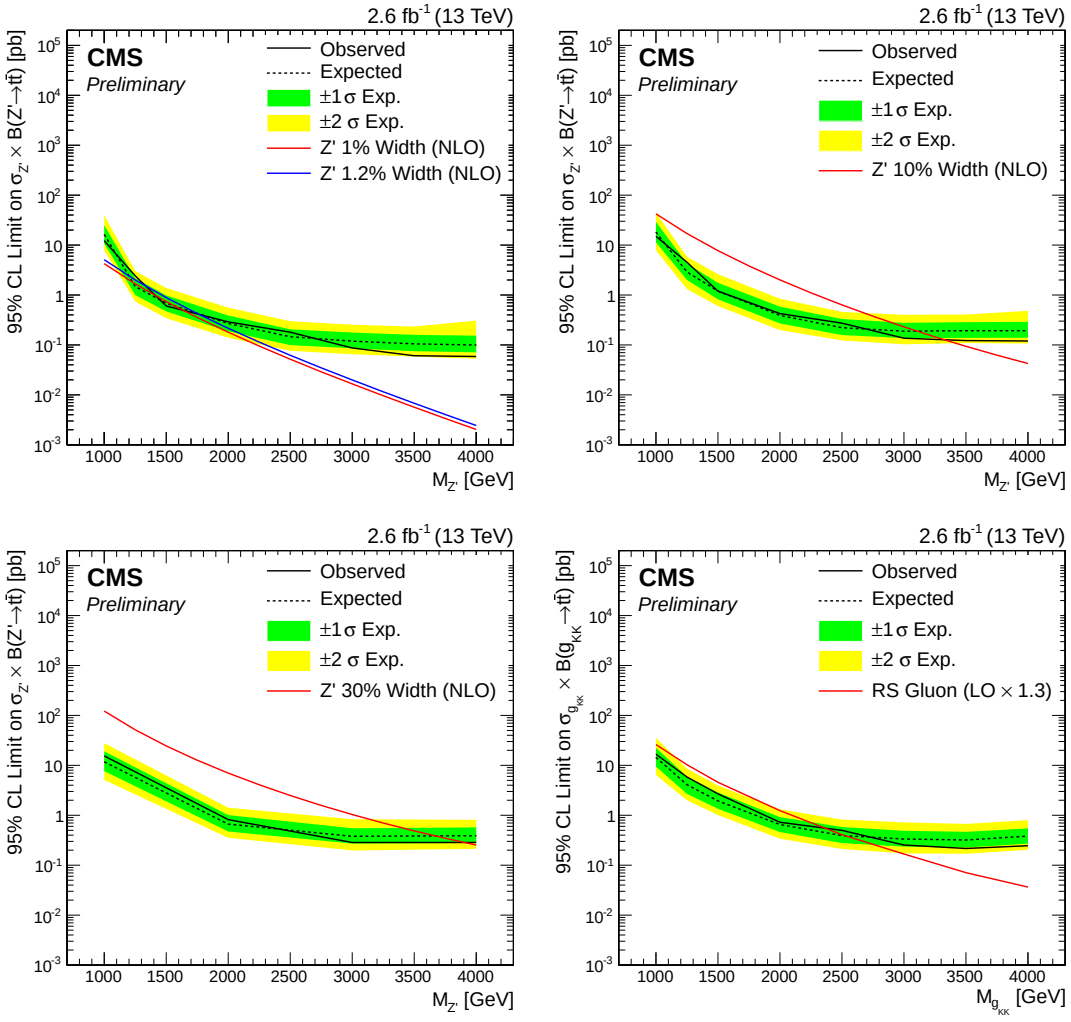

Figure 3: Expected and observed 95% CL upper limits on the cross section times branching ratio for the four signal models, as a function of the new heavy particle mass. The four models considered are a Z′ boson whose width is 1% of its mass (upper left), a 10% width Z′ boson (upper right), a 30% width Z′ boson (lower left), and an RS KK gluon (lower right). The solid (dashed) black line gives the observed (median expected) limits, while the one (two) sigma expected limit band is shown in green (yellow). The solid line shows the expected theoretical cross section for the signal process of interest.

Table 5: Table of expected and observed 95% CL cross section limits, for the wide (10% width) Z′ signal hypothesis.

Wide Z′ Signal Hypothesis

Mass (GeV)	Observed 95% CL Limit (pb)	Expected 95% CL Limits (pb)				
		-2σ	-1σ	Median	$+1\sigma$	$+2\sigma$
1000	**15**	7.8	11	**18**	29	44
1250	**4.5**	1.3	2.0	**2.9**	4.3	5.8
1500	**1.2**	0.6	0.82	**1.2**	1.8	2.6
2000	**0.42**	0.2	0.27	**0.39**	0.58	0.84
2500	**0.27**	0.12	0.16	**0.22**	0.33	0.46
3000	**0.14**	0.1	0.14	**0.19**	0.28	0.4
3500	**0.12**	0.11	0.14	**0.19**	0.29	0.41
4000	**0.12**	0.11	0.14	**0.19**	0.29	0.48

Table 6: Table of expected and observed 95% CL cross section limits, for the extra wide (30% width) Z′ signal hypothesis.

Z′ (30% Width) Signal Hypothesis

Mass (GeV)	Observed 95% CL Limit (pb)	Expected 95% CL Limits (pb)				
		-2σ	-1σ	Median	$+1\sigma$	$+2\sigma$
1000	**15**	5.1	7.7	**12**	19	28
2000	**0.82**	0.35	0.47	**0.66**	1	1.4
3000	**0.29**	0.2	0.27	**0.38**	0.55	0.83
4000	**0.28**	0.21	0.28	**0.39**	0.57	0.81

Table 7: Table of expected and observed 95% CL cross section limits, for the RS Gluon signal hypothesis.

RS Gluon Signal Hypothesis

Mass (GeV)	Observed 95% CL Limit (pb)	Expected 95% CL Limits (pb)				
		-2σ	-1σ	Median	$+1\sigma$	$+2\sigma$
1000	**17**	6.4	9.4	**14**	22	35
1250	**5.8**	2.0	2.7	**4.1**	6.0	8.6
1500	**2.7**	1.0	1.4	**1.9**	2.9	4.0
2000	**0.72**	0.34	0.46	**0.65**	0.92	1.3
2500	**0.5**	0.21	0.28	**0.39**	0.58	0.82
3000	**0.25**	0.17	0.24	**0.33**	0.49	0.72
3500	**0.22**	0.17	0.23	**0.32**	0.47	0.67
4000	**0.25**	0.20	0.27	**0.38**	0.55	0.8

References

[1] S. Dimopoulos and H. Georgi, "Softly Broken Supersymmetry and SU(5)", *Nucl. Phys. B* **193** (1981) 150, doi:10.1016/0550-3213(81)90522-8.

[2] S. Weinberg, "Implications of Dynamical Symmetry Breaking", *Phys. Rev. D* **13** (1976) 974, doi:10.1103/PhysRevD.13.974.

[3] L. Susskind, "Dynamics of Spontaneous Symmetry Breaking in the Weinberg- Salam Theory", *Phys. Rev. D* **20** (1979) 2619, doi:10.1103/PhysRevD.20.2619.

[4] C. T. Hill and S. J. Parke, "Top production: Sensitivity to new physics", *Phys. Rev. D* **49** (1994) 4454, doi:10.1103/PhysRevD.49.4454, arXiv:hep-ph/9312324.

[5] R. S. Chivukula, B. A. Dobrescu, H. Georgi, and C. T. Hill, "Top quark seesaw theory of electroweak symmetry breaking", *Phys. Rev. D* **59** (1999) 075003, doi:10.1103/PhysRevD.59.075003, arXiv:hep-ph/9809470.

[6] N. Arkani-Hamed, A. G. Cohen, and H. Georgi, "Electroweak symmetry breaking from dimensional deconstruction", *Phys. Lett. B* **513** (2001) 232, doi:10.1016/S0370-2693(01)00741-9, arXiv:hep-ph/0105239.

[7] N. Arkani-Hamed, S. Dimopoulos, and G. R. Dvali, "The hierarchy problem and new dimensions at a millimeter", *Phys. Lett. B* **429** (1998) 263, doi:10.1016/S0370-2693(98)00466-3, arXiv:hep-ph/9803315.

[8] L. Randall and R. Sundrum, "A large mass hierarchy from a small extra dimension", *Phys. Rev. Lett.* **83** (1999) 3370–3373, doi:10.1103/PhysRevLett.83.3370, arXiv:hep-ph/9905221.

[9] L. Randall and R. Sundrum, "An alternative to compactification", *Phys. Rev. Lett.* **83** (1999) 4690–4693, doi:10.1103/PhysRevLett.83.4690, arXiv:hep-th/9906064.

[10] J. Rosner, "Prominent Decay Modes of a Leptophobic Z"', *Phys. Rev. B* **387** (1996) 113–117, doi:10.1016/0370-2693(96)01022-2, arXiv:9607207v3.

[11] CDF Collaboration, "Cross Section for Topcolor Z' decaying to top-antitop", Technical Report FERMILAB-FN-0687, Fermilab, 1999. arXiv:9911288.

[12] K. Lynch, M. Narain, E. Simmons, and S. Mrenna, "Finding Z' bosons coupled preferentially to the third family at CERN LEP and the Fermilab Tevatron", *Phys. Rev. D* **63** (2001) 035006, doi:10.1103/PhysRevD.63.035006, arXiv:0007286.

[13] K. Agashe et al., "LHC signals for warped electroweak neutral gauge bosons", *Phys. Rev. D* **76** (2007) 115015, doi:10.1103/PhysRevD.80.075007, arXiv:0810.1497.

[14] K. Agashe et al., "LHC signals from warped extra dimensions", *Phys. Rev. D* **77** (2008) 015003, doi:10.1103/PhysRevD.77.015003, arXiv:0612015.

[15] A. Faraggi and M. Guzzi, "Extra Z's and W's in heterotic-string derived models", *Eur. Phys. J. C* **75** (2015) 537, doi:10.1140/epjc/s10052-015-3763-4, arXiv:1507.07406.

[16] T. Li, J. Maxin, V. Mayes, and D. Nanopoulos, "Diboson Excesses in Leptophobic $U(1)_{\rm LP}$ Models from String Theories", *Phys. Rev. D* **93** (2016) 045007, doi:10.1103/PhysRevD.93.045007, arXiv:1509.06821.

[17] CMS Collaboration, "Search for new physics in high mass diphoton events in proton-proton collisions at $\sqrt{s}$ = 13 TeV", CMS Physics Analysis Summary CMS-PAS-EXO-15-004, CERN, Geneva, 2016.

[18] CDF Collaboration, "Search for resonant production of $t\bar{t}$ pairs in 4.8 fb^{-1} of integrated luminosity of $p\bar{p}$ collisions at $\sqrt{s}$=1.96 TeV", *Phys. Rev. D* **84** (2011) 072004, doi:10.1103/PhysRevD.84.072004, arXiv:1107.5063.

[19] D0 Collaboration, "Search for $t\bar{t}$ Resonances in the Lepton+Jets Final State in $p\bar{p}$ Collisions at $\sqrt{s}$ = 1.96 TeV", *Phys. Rev. B* **668** (2008) 98–104, doi:10.1016/j.physletb.2008.08.027, arXiv:0804.3664.

[20] CMS Collaboration, "Search for anomalous $t\bar{t}$ production in the highly-boosed all-hadronic final state", *JHEP* **09** (2012) 29, doi:10.1007/JHEP09(2012)029, arXiv:1204.2488.

[21] CMS Collaboration, "Search for resonant $t\bar{t}$ production in lepton+jets events in pp collisions at $\sqrt{s}$ = 7 TeV", *JHEP* **12** (2012) 15, doi:10.1007/JHEP12(2012)015, arXiv:1209.4397.

[22] ATLAS Collaboration, "Search for resonances decaying into top-quark pairs using fully hadronic decays in pp collisions with ATLAS at $\sqrt{s}$ = 7 TeV", *JHEP* **01** (2013) 116, doi:10.1007/JHEP01(2013)116, arXiv:1211.2202.

[23] ATLAS Collaboration, "A search for $t\bar{t}$ resonances in lepton+jets events with highly-boosed top quarks collected in pp collisions with ATLAS at $\sqrt{s}$ = 7 TeV", *JHEP* **09** (2012) 41, doi:10.1007/JHEP09(2012)041, arXiv:1207.2409.

[24] CMS Collaboration, "Search for Anomalous Top Quark Pair Production in the Boosted All-Hadronic Final State using pp Collisions at $\sqrt{s} = 8$ TeV", CMS Physics Analysis Summary CMS-PAS-B2G-12-005, 2013.

[25] CMS Collaboration, "Searches for new physics using the $t\bar{t}$ invariant mass distribution in pp collisions at $\sqrt{s}$ = 8 TeV", *Phys. Rev. Lett.* **111** (2013) 211804, doi:10.1103/PhysRevLett.111.211804, arXiv:1309.2030.

[26] CMS Collaboration, "Search for resonant $t\bar{t}$ production in proton-proton collisions at $\sqrt{s}$ = 8 TeV", *Phys. Rev. D* **93** (2016) 012001, doi:10.1103/PhysRevD.93.012001, arXiv:1506.03062.

[27] ATLAS Collaboration, "A search for $t\bar{t}$ resonances using lepton-plus-jets events in proton-proton collisions at $\sqrt{s}$ = 8 TeV with the ATLAS detector", *JHEP* **08** (2015) 148, doi:10.1007/JHEP08(2015)148, arXiv:1505.07018.

[28] CMS Collaboration, "Search for $t\bar{t}$ resonances in boosted semileptonic final states in pp collisions at $\sqrt{s}$ = 13 TeV", CMS Physics Analysis Summary CMS-PAS-B2G-15-002, CERN, Geneva, 2016.

[29] ATLAS Collaboration Collaboration, "Search for heavy particles decaying to pairs of highly-boosted top quarks using lepton-plus-jets events in proton-proton collisions at $\sqrt{s}$ = 13 TeV with the ATLAS detector", ATLAS Conference Note ATLAS-CONF-2016-014, CERN, 2016.

[30] CMS Collaboration, "Top Tagging with New Approaches", CMS Physics Analysis Summary CMS-PAS-JME-15-002, 2016.

[31] M. Dasgupta, A. Fregoso, S. Marzani, and G. P. Salam, "Towards an understanding of jet substructure", *JHEP* **09** (2013) 029, doi:10.1007/JHEP09(2013)029, arXiv:1307.0007.

[32] J. Thaler and K. Van Tilburg, "Identifying Boosted Objects with N-subjettiness", *JHEP* **1103** (2011) 015, doi:10.1007/JHEP03(2011)015, arXiv:1011.2268.

[33] J. Thaler and K. Van Tilburg, "Maximizing Boosted Top Identification by Minimizing N-subjettiness", *JHEP* **1202** (2012) 093, doi:10.1007/JHEP02(2012)093, arXiv:1108.2701.

[34] CMS Collaboration, "Performance of b tagging at sqrt(s)=8 TeV in multijet, ttbar and boosted topology events", CMS Physics Analysis Summary CMS-PAS-BTV-13-001, 2013.

[35] CMS Collaboration, "The CMS experiment at the CERN LHC", *JINST* **3** (2008) S08004, doi:10.1088/1748-0221/3/08/S08004.

[36] CMS Collaboration, "Particle–Flow Event Reconstruction in CMS and Performance for Jets, Taus, and $E_{\mathrm{T}}^{\mathrm{miss}}$", *CMS Physics Analysis Summary* **CMS-PAS-PFT-09-001** (2009).

[37] CMS Collaboration, "Commissioning of the Particle-flow Event Reconstruction with the first LHC collisions recorded in the CMS detector",.

[38] M. Cacciari, G. P. Salam, and G. Soyez, "The anti-kt jet clustering algorithm", *JHEP* **04** (2008) 063, doi:10.1088/1126-6708/2008/04/063, arXiv:0802.1189.

[39] M. Cacciari and G. P. Salam, "Dispelling the N**3 myth for the k(t) jet-finder", *Phys. Lett. B* **641** (2006) 57, doi:10.1016/j.physletb.2006.08.037, arXiv:hep-ph/0512210.

[40] M. Cacciari, G. P. Salam, and G. Soyez, "FastJet user manual", *Eur.Phys.J. C* **72** (2012) 1896, doi:10.1140/epjc/s10052-012-1896-2, arXiv:1111.6097.

[41] M. Cacciari and G. P. Salam, "Pileup subtraction using jet areas", *Phys. Lett. B* **659** (2008) 119, doi:10.1016/j.physletb.2007.09.077, arXiv:0707.1378.

[42] CMS Collaboration, "Determination of jet energy calibration and transverse momentum resolution in CMS", *JINST* **6** (2011) P11002, doi:10.1088/1748-0221/6/11/P11002, arXiv:1107.4277.

[43] Y. L. Dokshitzer, G. D. Leder, S. Moretti, and B. R. Webber, "Better Jet Clustering Algorithms", *JHEP* **08** (1997) 001, doi:10.1088/1126-6708/1997/08/001, arXiv:hep-ph/9707323.

[44] M. Wobisch and T. Wengler, "Hadronization corrections to jet cross sections in deep-inelastic scattering", arXiv:hep-ph/9907280.

[45] A. J. Larkoski, S. Marzani, G. Soyez, and J. Thaler, "Soft Drop", *JHEP* **05** (2014) 146, doi:10.1007/JHEP05(2014)146, arXiv:1402.2657.

[46] CMS Collaboration, "Identification of b-quark jets with the CMS experiment", *JINST* **8** (2013) P04013, doi:10.1088/1748-0221/8/04/P04013, arXiv:1211.4462.

[47] J. Alwall et al., "The automated computation of tree-level and next-to-leading order differential cross sections, and their matching to parton shower simulations", *JHEP* **07** (2014) 079, doi:10.1007/JHEP07(2014)079, arXiv:1405.0301.

[48] T. Sjöstrand et al., "An Introduction to PYTHIA 8.2", *Comput. Phys. Commun.* **191** (2015) 159, doi:10.1016/j.cpc.2015.01.024, arXiv:1410.3012.

[49] M. L. Mangano, M. Moretti, F. Piccinini, and M. Treccani, "Matching Matrix Elements and Shower Evolution for Top-Quark Production in Hadronic Collisions", *JHEP* **01** (2007) 013, doi:10.1088/1126-6708/2007/01/013, arXiv:hep-ph/0611129.

[50] P. Nason, "A New method for combining NLO QCD with shower Monte Carlo algorithms", *JHEP* **11** (2004) 040, doi:10.1088/1126-6708/2004/11/040, arXiv:hep-ph/0409146.

[51] S. Frixione, P. Nason, and C. Oleari, "Matching NLO QCD computations with Parton Shower simulations: the POWHEG method", *JHEP* **11** (2007) 070, doi:10.1088/1126-6708/2007/11/070, arXiv:0709.2092.

[52] S. Alioli, P. Nason, C. Oleari, and E. Re, "A general framework for implementing NLO calculations in shower Monte Carlo programs: the POWHEG BOX", *JHEP* **06** (2010) 043, doi:10.1007/JHEP06(2010)043, arXiv:1002.2581.

[53] S. Frixione, P. Nason, and G. Ridolfi, "A Positive-weight next-to-leading-order Monte Carlo for heavy flavour hadroproduction", *JHEP* **09** (2007) 126, doi:10.1088/1126-6708/2007/09/126, arXiv:0707.3088.

[54] E. Re, "Single-top Wt-channel production matched with parton showers using the POWHEG method", *Eur. Phys. J. C* **71** (2011) 1547, doi:10.1140/epjc/s10052-011-1547-z, arXiv:1009.2450.

[55] M. Czakon and A. Mitov, "Top++: A Program for the Calculation of the Top-Pair Cross-Section at Hadron Colliders", *Comput. Phys. Commun.* **185** (2014) 2930, doi:10.1016/j.cpc.2014.06.021, arXiv:1112.5675.

[56] NNPDF Collaboration, "Parton distributions for the LHC Run II", *JHEP* **04** (2015) 040, doi:10.1007/JHEP04(2015)040, arXiv:1410.8849.

[57] CMS Collaboration, "Event generator tunes obtained from underlying event and multiparton scattering measurements", *Eur. Phys. J. C* **76** (2016), no. 3, 155, doi:10.1140/epjc/s10052-016-3988-x, arXiv:1512.00815.

[58] CMS Collaboration, "Measurement of the differential cross section for top quark pair production in pp collisions at sqrt(s) = 8 TeV", (2015). arXiv:1505.04480.

[59] J. Ott. http://www.theta-framework.org.

[60] R. Bonciani, T. Jezo, M. Klasen, F. Lyonnet, I. Schienbein, "Electroweak top-quark pair production at the LHC with Z' bosons to the NLO QCD in POWHEG", *JHEP* **02** (2016) 141, doi:10.1007/JHEP02(2016)141, arXiv:1511.08185.